

# Single-photon imager based on a superconducting nanowire delay line

Qing-Yuan Zhao<sup>1</sup>, Di Zhu<sup>1</sup>, Niccolò Calandri<sup>1,2</sup>, Andrew E. Dane<sup>1</sup>, Adam N. McCaughan<sup>1</sup>, Francesco Bellei<sup>1</sup>, Hao-Zhu Wang<sup>1</sup>, Daniel F. Santavicca<sup>3</sup> and Karl K. Berggren<sup>1\*</sup>

Detecting spatial and temporal information of individual photons is critical to applications in spectroscopy, communication, biological imaging, astronomical observation and quantum-information processing. Here we demonstrate a scalable single-photon imager using a single continuous superconducting nanowire that is not only a single-photon detector but also functions as an efficient microwave delay line. In this context, photon-detection pulses are guided in the nanowire and enable the readout of the position and time of photon-absorption events from the arrival times of the detection pulses at the nanowire's two ends. Experimentally, we slowed down the velocity of pulse propagation to ~2% of the speed of light in free space. In a 19.7 mm long nanowire that meandered across an area of  $286 \times 193 \mu\text{m}^2$ , we were able to resolve ~590 effective pixels with a temporal resolution of 50 ps (full width at half maximum). The nanowire imager presents a scalable approach for high-resolution photon imaging in space and time.

Currently, quantum optics is limited by our ability to sense and process efficiently information about single photons. For example, to enhance the information-carrying capacity of a quantum channel<sup>1</sup> and improve security in quantum-key distribution<sup>2,3</sup>, information is typically encoded in the position and arrival time of individual photons. To determine the spatial and temporal information of photons is currently accomplished by single-photon detector (SPD) arrays. Among existing SPD array technologies, the transition-edge sensor (TES) and the microwave kinetic inductance detector (MKID) provide moderate spectral information, but less-impressive temporal resolution (for example, the timing uncertainty, or jitter, is measured in nanoseconds for TESs<sup>4</sup> and microseconds for MKIDs<sup>5</sup>). Photomultiplier tubes and single-photon avalanche diodes have sub 1 ns timing jitters in the visible domain, but their detection performance deteriorates in the infrared region, and scaling these technologies to large spatial arrays is challenging<sup>6</sup>. Improved timing performance of sub 20 ps timing jitter<sup>7</sup> and sub 10 ns recovery time<sup>8</sup> is possible with superconducting-nanowire single-photon detectors (SNSPDs), which also have been demonstrated to have a near-unity detection efficiency<sup>9</sup>, less than one dark-count per second (c.p.s.)<sup>10</sup>, a wide spectral response from the visible to the infrared region<sup>11</sup> and greater than  $10^8$  c.p.s. counting rate<sup>12</sup>. However, attempts to create arrays of SNSPDs have had limited success<sup>13–18</sup>. Traditional row–column rectangular pixel arrays require large numbers of readout lines<sup>15</sup>, whereas attempts at time-based and frequency-based multiplexing architectures require additional components within and between pixels, and thus suffer from low fill factors<sup>16,18</sup>. Consequently, the current state-of-the-art SNSPD array is limited to ~100 pixels<sup>15</sup>.

The typical operation of an SNSPD lacks spatial sensitivity, although the excitation caused by the absorption of a photon is localized within the nanowire. In the simplest broadly accepted detection model of an SNSPD<sup>19</sup>, an absorbed photon generates a localized region of elevated electron temperature, that is, a hotspot, which leads to the formation of a resistive domain across the nanowire. Unfortunately, the conventional electrical readout of an SNSPD

could not be used to determine the location of the resistive domain because, electrically, the nanowire was modelled as a lumped-element inductor in series with a nonlinear dynamic resistor that represented the resistive domain<sup>20</sup>. In such a scheme, the relative location of the resistor and inductor cannot change the output behaviour of the circuit. For very long nanowires, in which the length exceeds the wavelength of the readout signal, this lumped-element model no longer fully describes the device behaviour. In such situations, a distributed-element model must be used<sup>21,22</sup>.

Here we describe an experiment in which we used a superconducting nanowire as the centre conductor in a microwave coplanar transmission line to determine the position of the hotspot along the nanowire while simultaneously preserving information about the time of arrival of the photon. This approach uses a continuous nanowire to realize a scalable single-photon imager, which we refer to as a superconducting-nanowire single-photon imager (SNSPI) to distinguish it from an SNSPD. A sketch of the SNSPI is shown in Fig. 1a. The superconducting nanowire in an SNSPI is not only designed as a single-photon-sensitive detector, but also functions as a microwave delay line that displays ultralow velocity (~2% of the speed of light in free space). Therefore, a relatively small propagation distance results in a measurable time delay<sup>21,23</sup>. The nanowire is terminated at each end with a Klopfenstein taper to transform from the high characteristic impedance of the nanowire to  $50 \Omega$  (ref. 24). This ensures an efficient coupling of the electrical pulses triggered by a photon-detection event to a  $50 \Omega$  microwave readout circuit, which in turn allows us to extract the time and position of the absorbed photon using the relative arrival times of the output electrical pulses at the two ends of the nanowire.

## Guiding microwaves in a superconducting nanowire

The low signal-propagation velocity in an SNSPI results from the kinetic inductance of a thin superconducting nanowire. In a two-fluid model, the superconducting electrons move without resistance and have a kinetic energy of  $\frac{1}{2}n_s mv_s^2$  ( $n_s$  is the superconducting

<sup>1</sup>Department of Electrical Engineering and Computer Science, Massachusetts Institute of Technology, Cambridge, Massachusetts 02139, USA. <sup>2</sup>Department of Electronics, Information and Bioengineering, Politecnico di Milano, Milano 22020, Italy. <sup>3</sup>Department of Physics, University of North Florida, Jacksonville, Florida 32224, USA. \*e-mail: [berggren@mit.edu](mailto:berggren@mit.edu)

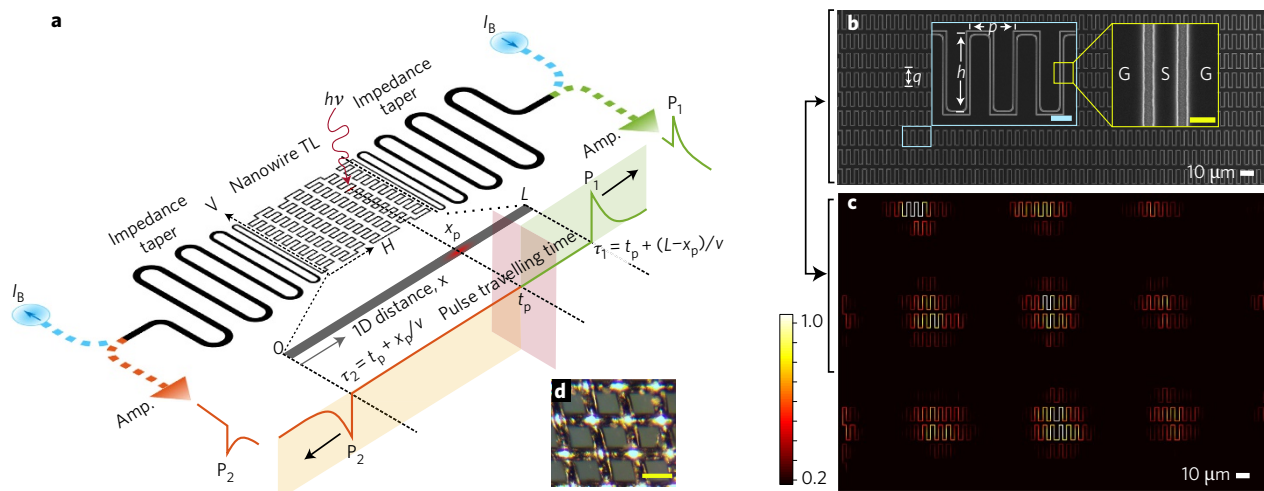


**Figure 1 | SNSPI.** **a**, Architecture of the SNSPI. The nanowire transmission line (TL) and the impedance tapers were fabricated in coplanar-waveguide structures (the ground plane is not shown in the sketch).  $P_1$  and  $P_2$ , detection pulses from the two ends. Amp., radiofrequency amplifier. **b**, A scanning electron micrograph of the top nine rows of the meandered nanowire (out of 15 rows in total). The dimensions shown are  $q = 13.0 \mu\text{m}$ ,  $h = 9.7 \mu\text{m}$  and  $p = 5.4 \mu\text{m}$ . Inset scale bars,  $2 \mu\text{m}$  (left) and  $300 \text{ nm}$  (right). **c**, A single-photon image of the pattern formed by light passing through a metal mesh, which was placed on top of the SNSPI with a gap of  $\sim 200 \mu\text{m}$  (Supplementary Information gives the imaging set-up). The circular periodic patterns reflect the opening holes of the mesh. The wavelength of the light was  $780 \text{ nm}$ . The image consists of data from 427,905 photon-detection events. The colour of the map shows the normalized photon counts at each location. **d**, An optical micrograph of the metal mesh with an opening size of  $43 \mu\text{m}$  and a wire diameter of  $30 \mu\text{m}$ . Scale bar,  $50 \mu\text{m}$ .

electron density,  $m$  is the electron mass and  $v_s$  is the velocity of the Cooper pairs). Alternatively, driving the superconducting electrons can be seen as kinetic inductivity, which is expressed as  $\mathcal{L}_k = m/n_s e^2 = \mu_0 \lambda_L^2$  ( $e$  is the elementary charge,  $\lambda_L$  is the London penetration depth and  $\mu_0$  is the permeability). In our experiments, the superconducting nanowire patterned from a  $\sim 7 \text{ nm}$  thick niobium nitride film has kinetic inductivity  $\mathcal{L}_k = 3.43 \times 10^{-19} \text{ Hm}$ , which is larger than its Faraday inductivity by two orders of magnitude. An alternative way to study wave propagation in the superconducting nanowire is to consider the nanowire as a plasmonic material (Supplementary Information)<sup>25,26</sup>.

To guide the detection pulses, we designed the nanowire into a coplanar waveguide (CPW) structure (its dimensions are given in Fig. 1b). The signal propagation velocity is  $v = 1/\sqrt{L_s C_s}$  and the characteristic impedance is  $Z = \sqrt{L_s/C_s}$  where  $L_s$  and  $C_s$  are the inductance and capacitance per unit length, respectively. As we mentioned above, the kinetic inductance is much higher than the Faraday inductance in a superconducting nanowire. Therefore, there is a significant reduction of  $v_s$  and an increase of  $Z$  compared with the same structure made from normal metals (simulation results are discussed in Methods). Experimentally, the measured velocity in the SNSPI for imaging demonstrations was  $5.56 \mu\text{m ps}^{-1}$ . This microwave modification implies that a photon-sensitive nanowire can function as an efficient delay line in which photon-detection pulses have to propagate along the nanowire for a time determined by the photon-detection position.

### Operating principle of an SNSPI

The operation of the SNSPI is shown in Fig. 1a. After a photon is absorbed at location  $x_p$  and at time  $t_p$ , the increase of local resistance generates two electrical pulses,  $P_1$  and  $P_2$ , of opposite polarities, which propagate with a constant velocity  $v$  towards the two ends of the transmission line and introduce delays  $\tau_1$  and  $\tau_2$ , respectively. After removing the fixed delays from the tapers, cables and readout electronics and extracting  $\tau_1$  and  $\tau_2$  from the arrival times of the electrical pulses, every  $(x_p, t_p)$  pair can be determined by using two linear functions:  $x_p = ((\tau_2 - \tau_1)v + L)/2$  and  $t_p = ((\tau_2 + \tau_1) - L/v)/2$ , where  $L$  is the total length of the nanowire. Such a delay-based

readout is conceptually similar to the readout of a time-multiplexed SNSPD array<sup>16</sup> and has also been applied in microchannel-plate detectors<sup>27</sup>. However, the SNSPI simultaneously acts as a detector and delay component, without any multiplexing circuits or clock signals, which results in a dramatically more-compact design that is suitable for large-scale integration. Compared with single-pixel-based imaging technology that uses compressing sampling methods to reconstruct an image<sup>28</sup>, the SNSPI images photons that are directly projected or emitted from the object, which avoids additional coupling loss and resolution degeneration during the spatial modulation of incident light. Thus, SNSPIs should be characterized by a higher imaging speed, a higher spatial resolution and a simpler apparatus compared with a single-pixel camera based on SNSPDs<sup>29</sup>.

### Single-photon-imaging performance

To create a 2D image with horizontal and vertical addresses ( $H, V$ ), the one-dimensional (1D) nanowire is meandered to cover a 2D area. The spatial resolution in each direction could thus be optimized independently for particular applications (for example, near-field imaging at subwavelength resolution by reducing the spacing between adjacent sections of the nanowire). In our experiments, as shown in Fig. 1b, the nanowire was meandered in both the  $H$  direction and the  $V$  direction to have nearly equal spatial resolution in  $H$  and  $V$ . This double-meandered nanowire covers a rectangular area of  $286 \times 193 \mu\text{m}^2$ . To demonstrate the imaging process, we placed an object on top of this rectangular area and evenly illuminated the double-meandered nanowire through the object to project a pattern on the nanowire (Methods). Figure 1c shows an image of a metal mesh with a simple periodic structure in which opening holes correspond to the visible grid of circular patterns. Figure 2 shows the image construction formed by 989,897 photon-detection events. A video (Supplementary Information) also demonstrates how the accumulation of detection events generated the image. In the present set-up, the imaging time was limited by the acquisition speed of the oscilloscope, which had a refresh rate of only  $\sim 100$  waveforms per second. Consequently, most of the detection pulses from the SNSPI were not recorded. To investigate

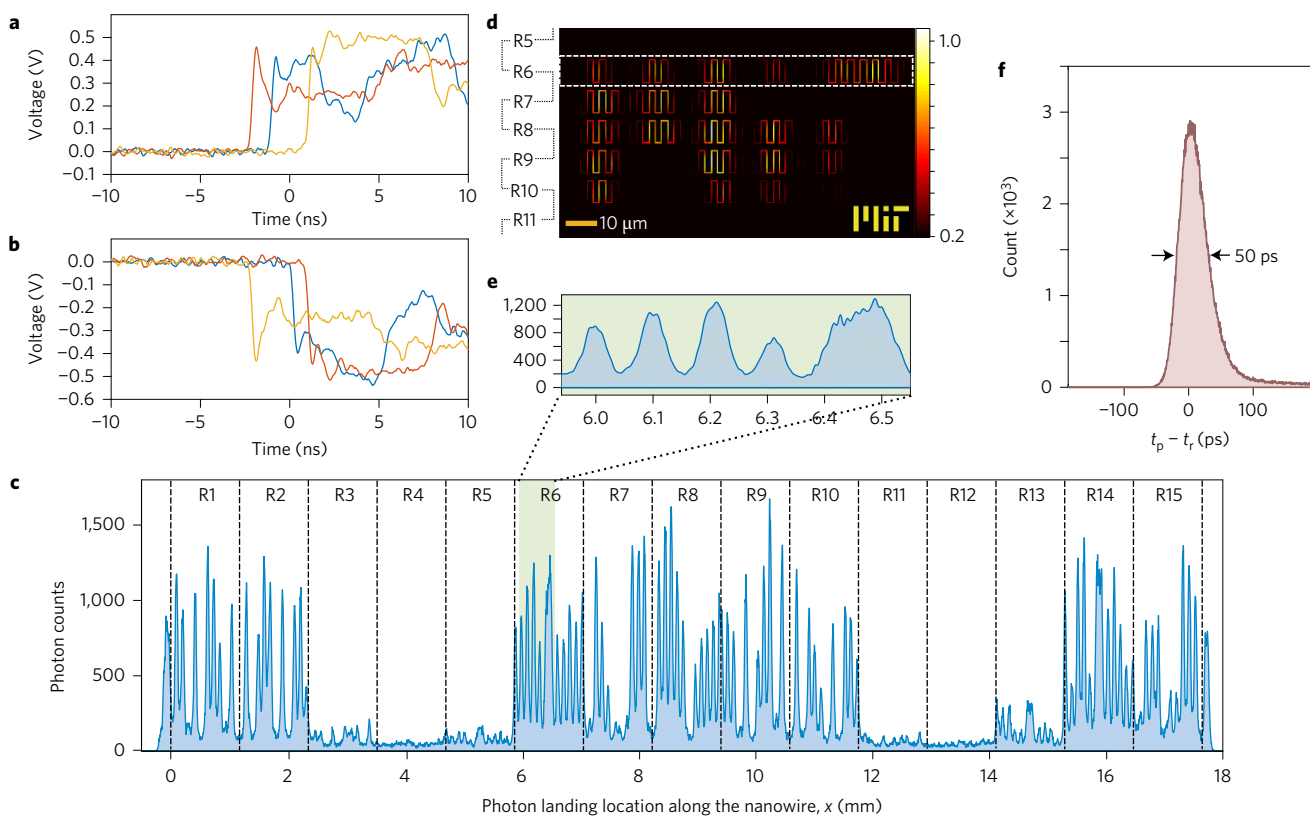


**Figure 2 | Spatial and temporal detection by the SNSPI.** **a,b,** Oscilloscope waveforms of output pulses from the two ends of the nanowire. We selected three pulse pairs whose arrival times corresponded to three different photon-detection locations. The device was illuminated with sub-picosecond optical pulses from a mode-locked laser at a wavelength of 1.5  $\mu\text{m}$ . **c,** Histogram of 989,897 photon detections for imaging an array of institutional logos. The x axis is the position along the nanowire. A continuous-wave light-emitting diode source at 405 nm was used to project the object on the imager. The span of  $x$  was divided into 15 sections that correspond to the 15 rows (R1–R15) of the double-meandered nanowire. **d,** Image of one institutional logo constructed from the photon-position data (only a portion of the full image region is shown). **e,** Magnified section of the histogram that corresponds to the bright lines included within the green-shaded area in R6. **f,** Histogram of the difference between the photon-arrival time  $t_p$  measured by the SNSPI and a reference time  $t_r$ . We used a 1.5  $\mu\text{m}$  mode-locked laser to illuminate the SNSPI and generate  $t_r$  with picosecond resolution. The FWHM of the histogram profile was 50 ps, which was used to define the timing jitter  $j_d$ .

the ultimate speed of the SNSPI, we ignored the timing information of the pulse and only counted pulses from the SNSPI using a 200 MHz counter, and also removed the charging effects from the amplifier<sup>30</sup> (Methods gives the maximum counting rate ( $CR_{\max}$ ) characterization). We defined  $CR_{\max}$  as the count rate when the average detection efficiency dropped by half, which was  $2 \times 10^6$  c.p.s. measured for photons at a wavelength of 1.5  $\mu\text{m}$ , indicating an estimated imaging time of a few seconds to construct the same image of Fig. 1c if the data processing set-up were improved.

The spatial resolution of the imager was dominated by the electrical noise in the readout circuits and the speed of signal propagation in the transmission line. Consider a photon arriving at  $x_p$  that results in pulses observed at times  $\tau_1$  and  $\tau_2$ . Electrical noise contributed to the variation in the determination of  $\tau_1$  and  $\tau_2$ , which results in a variation of the measured  $x_p$  based on the function  $x_p = ((\tau_2 - \tau_1)v + L)/2$ . We quantified this uncertainty by defining a Gaussian point-spread function  $b(x) = \exp(-x^2/2h^2)$  where  $h = (\delta/\rho) \times v/2$  ( $\delta$  is the standard deviation of the Gaussian distribution of electrical noise and  $\rho$  is the slope of the pulses at the discrimination threshold level). The point-spread function can be used to estimate the effective resolution as limited by electrical noise. From the waveform of the output pulses,  $(\delta/\rho)$ , which was characterized as the system's electrical jitter  $j_e$ , was determined to be 4.3 ps (Methods). Substituting the measured value of  $v = 5.6 \mu\text{m ps}^{-1}$  into the point-spread function  $b(x)$ , we have  $h = 12.0 \mu\text{m}$ , and the full width at half maximum (FWHM)  $f_w$  of  $b(x)$  is 28.4  $\mu\text{m}$ . The width of  $b(x)$  determines the noise-limited

spatial resolution, which is later compared with the measured width of the sharp peaks generated from dark counts.

Given the point-spread function defined above, the 2D spatial resolution can be calculated by taking into account the meander geometry, from which the position along the nanowire  $x$  is mapped to the 2D location  $(H,V)$ . In the geometry shown in Fig. 1b, the vertical spatial resolution is the spacing between rows  $q = 13.0 \mu\text{m}$  and the horizontal spatial resolution is  $f_w \times p/l_m = 6.9 \mu\text{m}$ , where  $l_m = 22.24 \mu\text{m}$  is the effective length of one meander period in each row. With these values of spatial resolution, we were able to image letters with a 12.6  $\mu\text{m}$  stroke width and 12.6  $\mu\text{m}$  spacing between the strokes (Fig. 2d). A smaller  $h$  could be achieved by reducing  $j_e$  or slowing down  $v$  even further by using other superconducting materials with a higher kinetic inductance (for example, tungsten silicide), substrates with higher dielectric constant (for example, LaAlO<sub>3</sub>) or other transmission-line structures (for example, microstrip lines).

The photon-arrival time  $t_p$  was determined using the equation  $t_p = ((\tau_2 + \tau_1) - L/v)/2$ . The temporal resolution was characterized by the timing jitter  $j_d$ , defined as the time variation of the measured photon-arrival times, which included both the electronic jitter from the noise and the intrinsic jitter from the photon-detection mechanism. To measure  $j_d$  precisely, we used a mode-locked laser at a wavelength of 1.5  $\mu\text{m}$  with an output split into two beams. One beam was attenuated to single-photon level and then sent to the SNSPI to measure  $t_p$ , whereas the other beam was measured by a fast

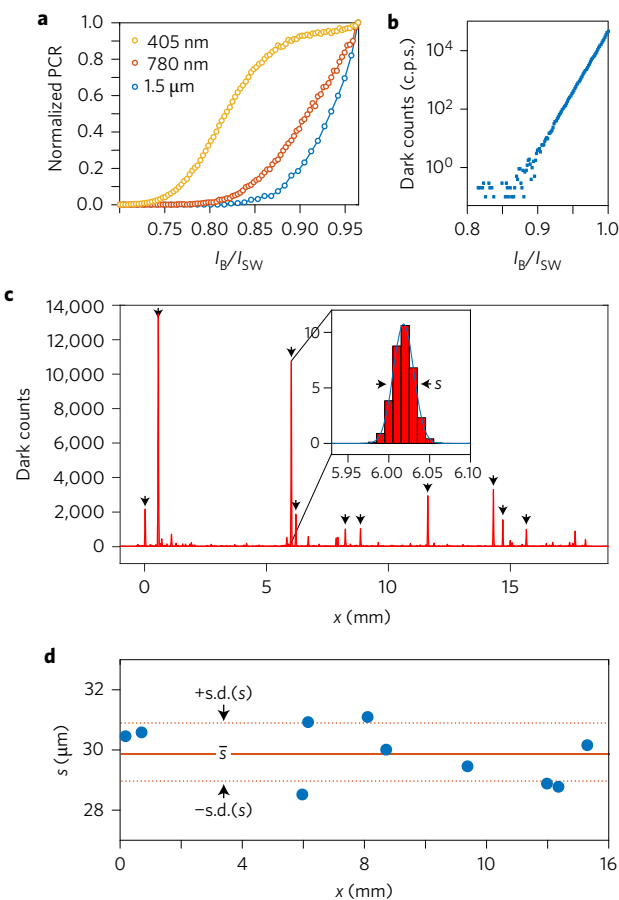


**Figure 3 | Detection performance of the SNSPI.** **a**, Photon count rate (PCR) versus  $I_B$  at wavelengths from visible to infrared. The traces are normalized to the photon counts at 65  $\mu$ A, where dark counts are  $1 \times 10^3$  c.p.s., to limit the error in the measurement of net photon counts. The x axis is normalized to  $I_{SW}$  (67.4  $\mu$ A). **b**, Overall dark counts versus  $I_B$ . **c**, Histogram of dark counts along the nanowire at  $I_B = 65 \mu$ A. We selected the ten peaks with the highest amplitudes (indicated by the arrows above the peaks) and fit each of them with a Gaussian function, of which we then calculated the FWHM  $s$ . **d**, Distribution of  $s$  from the considered ten peaks, marked as the blue dots. The average of  $s$  is  $\bar{s} = 29.9 \mu\text{m}$  and the with  $s.d.(s) = 0.9 \mu\text{m}$ .

photodiode to determine a timing reference  $t_r$  with picosecond resolution. Figure 2f shows the histogram of  $t_p - t_r$ . The FWHM of the histogram profile provided the timing jitter, which is  $j_d = 50 \text{ ps}$ . This value is consistent with reported timing jitters for SNSPDs and is significantly lower than the timing jitters of TESs and MKIDs.

The SNSPI also exhibited the wide optical bandwidth typical of conventional SNSPDs<sup>11</sup>. Figure 3a shows the photon counts versus bias current ( $I_B$ ) at wavelengths of 405 nm, 780 nm and 1.5  $\mu$ m. At 405 nm, the internal quantum efficiency of the wire saturated, which suggests a near-unity internal quantum efficiency for the nanowire. At longer wavelengths, the quantum efficiency was reduced, as would be expected for wires that are 300 nm wide. The ground plane in the coplanar structure limited the maximum light absorbance of the nanowire to be  $\sim 10\%$ . Future improvement of the detection efficiency requires a narrower nanowire of high internal efficiency and an optimized structure of both slow signal velocity and high optical absorbance. For example, a microstrip line integrated in an optical cavity can have a light absorption over 50% (simulation results are given in the Supplementary Information). As with the SNSPDs, the SNSPI will be sensitive to the polarization of the incident light. This sensitivity can be tuned by optimizing the wiring geometry or adding an integrated optical cavity<sup>31,32</sup>.

A spatial map of dark counts for the SNSPI can be created by operating the device in a well-shielded environment with no illumination (the dark count maps are discussed in the Supplementary Information). As shown in Fig. 3b, the total number of dark-count events summed over the length of the SNSPI exhibited an exponential dependence on the  $I_B$  that is similar to that measured in SNSPDs. The single-photon images obtained with the SNSPI were produced at a  $I_B$  of 60  $\mu$ A where the overall dark count rate was  $\sim 1$  c.p.s., thus ensuring a high signal-to-noise ratio for the images.

Measuring the distribution of dark counts with respect to nanowire coordinate offers an alternative method to characterize the spatial resolution of the SNSPI. To investigate the distribution of dark counts along the nanowire, we increased the  $I_B$  to 65  $\mu$ A to have more dark counts and thus reduce the overall acquisition time. Figure 3c shows the histogram of dark counts observed along the nanowire. We then calculated the FWHM  $s$  for each of the ten peaks with the highest amplitudes. The average value of  $s$  was  $\bar{s} = 29.9 \mu\text{m}$  and the variation was  $s.d.(s) = 0.9 \mu\text{m}$ . The considered ten peaks contributed to 74% of the total dark counts, whereas their combined length was only  $\sim 2\%$  of the total length of the nanowire, which indicates that the image quality is robust against dark counts. Dark counts could also be partially subtracted from the imager based on calibration from zero-light experiments.

The widths of the dark-count peaks were slightly larger than the spatial resolution calculated from the point-spread function, which suggests a possible intrinsic length of dark-count locations, or perhaps an underestimate of the system's electrical noise. To estimate the number of resolvable locations in the SNSPI, we used the measured  $\bar{s}$  as the minimum length that the SNSPI could distinguish. With this assumption, the maximum resolvable number of pixels  $N_p$  in the SNSPI is  $N_p = L_e/\bar{s} \cong 590$ , where  $L_e = 17.635 \text{ mm}$  is the effective length of a straight wire converted from the double-meandered geometry, taking into account the increase of the signal velocity at the corners. The estimated pixel density was thus  $\sim 10^6$  pixels  $\text{cm}^{-2}$ . The distribution of dark counts can also help us investigate where the dark counts originate, that is, whether the measured dark counts are determined by the constrictions of the nanowire or by the bends of the meandered wire<sup>33</sup> (Supplementary Information contains dark count images).

## Conclusion

In summary, we have introduced a scalable architecture for single-photon imagers with precise temporal resolution. By engineering the microwave behaviour of a photon-sensitive nanowire into a delay line with a slow velocity equal to 2% of the speed of light in free space, we demonstrated  $\sim 590$  effective pixels, sub 20  $\mu\text{m}$  spatial resolution and 50 ps FWHM temporal resolution in a 19.7 mm long superconducting nanowire. Given the reduced requirements for readout lines, the number of pixels and the image area could be further scaled up by integrating multiple SNSPIs into an SNSPI array with an on-chip readout to extract the delay information of the photon-detection pulses. The image quality could be enhanced further thanks to improved optics used to focus the object image, as well as electronics with a lower noise and a higher acquisition speed. With these improvements, we expect the SNSPI to become a powerful single-photon-detection tool in areas such as quantum information science, communications, single-photon imaging and spectroscopy, and even in astronomical observation.

## Methods

Methods and any associated references are available in the online version of the paper.

Received 28 July 2016; accepted 17 February 2017;  
published online 27 March 2017; corrected after print 14 August 2017

## References

- Zhang, L., Silberhorn, C. & Walmsley, I. A. Secure quantum key distribution using continuous variables of single photons. *Phys. Rev. Lett.* **100**, 1–4 (2008).
- Walborn, S. P., Lemelle, D. S., Almeida, M. P. & Ribeiro, P. H. S. Quantum key distribution with higher-order alphabets using spatially encoded qudits. *Phys. Rev. Lett.* **96**, 1–4 (2006).
- Mirhosseini, M. *et al.* High-dimensional quantum cryptography with twisted light. *New J. Phys.* **17**, 033033 (2015).
- Lamas-Linares, A. *et al.* Nanosecond-scale timing jitter for single photon detection in transition edge sensors. *Appl. Phys. Lett.* **102**, 231117 (2013).
- Gao, J. *et al.* A titanium-nitride near-infrared kinetic inductance photon-counting detector and its anomalous electrodynamics. *Appl. Phys. Lett.* **101**, 142602 (2012).
- Hadfield, R. H. Single-photon detectors for optical quantum information applications. *Nat. Photon.* **3**, 696–705 (2009).
- You, L. *et al.* Jitter analysis of a superconducting nanowire single photon detector. *AIP Adv.* **3**, 72135 (2013).
- Kerman, A. J., Rosenberg, D., Molnar, R. J. & Dauler, E. A. Readout of superconducting nanowire single-photon detectors at high count rates. *J. Appl. Phys.* **113**, 144511 (2013).
- Marsili, F. *et al.* Detecting single infrared photons with 93% system efficiency. *Nat. Photon.* **7**, 210–214 (2013).
- Yang, X. *et al.* Superconducting nanowire single photon detector with on-chip bandpass filter. *Opt. Express* **22**, 16267–16272 (2014).
- Marsili, F. *et al.* Efficient single photon detection from 500 nanometer to 5 micron wavelength. *Nano Lett.* **12**, 4799–4804 (2012).
- Rosenberg, D., Kerman, A. J., Molnar, R. J. & Dauler, E. A. High-speed and high-efficiency superconducting nanowire single photon detector array. *Opt. Express* **21**, 1440–1447 (2013).
- Zhao, Q. *et al.* Superconducting-nanowire single-photon-detector linear array. *Appl. Phys. Lett.* **103**, 142602 (2013).
- Miki, S., Yamashita, T., Wang, Z. & Terai, H. A 64-pixel NbTiN superconducting nanowire single-photon detector array for spatially resolved photon detection. *Opt. Express* **22**, 7811–7820 (2014).
- Allman, M. S. *et al.* A near-infrared 64-pixel superconducting nanowire single photon detector array with integrated multiplexed readout. *Appl. Phys. Lett.* **106**, 192601 (2015).
- Hofherr, M. *et al.* Time-tagged multiplexing of serially biased superconducting nanowire single-photon detectors. *IEEE Trans. Appl. Supercond.* **23**, 2501205 (2013).
- Hofherr, M. *et al.* Orthogonal sequencing multiplexer for superconducting nanowire single-photon detectors with RSFQ electronics readout circuit. *Opt. Express* **20**, 28683–28697 (2012).
- Doerner, S., Kuzmin, A., Wuensch, S., Ilin, K. & Siegel, M. Operation of superconducting nanowire single-photon detectors embedded in lumped-element resonant circuits. *IEEE Trans. Appl. Supercond.* **26**, 2200205 (2016).
- Gol'tsman, G. N. *et al.* Picosecond superconducting single-photon optical detector. *Appl. Phys. Lett.* **79**, 705–707 (2001).
- Yang, J. K. W. *et al.* Modeling the electrical and thermal response of superconducting nanowire single-photon detectors. *IEEE Trans. Appl. Supercond.* **17**, 581–585 (2007).
- Santavicca, D. F., Adams, J. K., Grant, L. E., McCaughan, A. N. & Berggren, K. K. Microwave dynamics of high aspect ratio superconducting nanowires studied using self-resonance. *J. Appl. Phys.* **119**, 234302 (2016).
- Calandri, N., Zhao, Q.-Y., Zhu, D., Dane, A. & Berggren, K. K. Superconducting nanowire detector jitter limited by detector geometry. *Appl. Phys. Lett.* **109**, 152601 (2016).
- Pond, J., Claassen, J. & Carter, W. Kinetic inductance microstrip delay lines. *IEEE Trans. Magn.* **23**, 903–906 (1987).
- Klopfenstein, R. W. A transmission line taper of improved design. *Proc. IRE* **44**, 31–35 (1956).
- Tsiatras, A., Fedotov, V. A., García de Abajo, F. J. & Zheludev, N. I. Low-loss terahertz superconducting plasmonics. *New J. Phys.* **14**, 115006 (2012).
- Majedi, A. H. Theoretical investigations on THz and optical superconductive surface plasmon interface. *IEEE Trans. Appl. Supercond.* **19**, 907–910 (2009).
- Jagutzki, O. *et al.* A broad-application microchannel-plate detector system for advanced particle or photon detection tasks: large area imaging, precise multi-bit timing information and high detection rate. *Nucl. Instrum. Methods Phys. Res. A* **477**, 244–249 (2002).
- Duarte, M. F. *et al.* Single-pixel imaging via compressive sampling. *IEEE Signal Process. Mag.* **25**, 83–91 (2008).
- Gerrits, T. *et al.* Progress toward a high-resolution single-photon camera based on superconducting single photon detector arrays and compressive sensing. In *Conf. Lasers and Electro-Optics (CLEO) STh30* (Optical Society of America, 2015).
- Zhao, Q. *et al.* Counting rate enhancements in superconducting nanowire single-photon detectors with improved readout circuits. *Opt. Lett.* **39**, 1869–1872 (2014).
- Dorenbos, S. N. *et al.* Superconducting single photon detectors with minimized polarization dependence. *Appl. Phys. Lett.* **93**, 161102 (2008).
- Zheng, F. *et al.* Design of efficient superconducting nanowire single photon detectors with high polarization sensitivity for polarimetric imaging. *J. Opt. Soc. Am. B* **33**, 2256–2264 (2016).
- Gaudio, R., op 't Hoog, K. P. M., Zhou, Z., Sahin, D. & Fiore, A. Inhomogeneous critical current in nanowire superconducting single-photon detectors. *Appl. Phys. Lett.* **105**, 222602 (2014).

## Acknowledgements

We thank R. Hobbs, C.-S. Kim and M. Mondol for their technical support in nanofabrication, and P. Mauskopf, J.K.W. Yang, Z. Zhang and E. Toomey for scientific discussion. This research was supported by the National Science Foundation (NSF) grants under contract no. ECCS-1509486 (Massachusetts Institute of Technology (MIT)) and no. ECCS-1509253 (University of North Florida) and the Air Force Office of Scientific Research grant under contract no. FA9550-14-1-0052. D.Z. is supported by a National Science Scholarship from A\*STAR, Singapore. N.C. thanks the Roberto Rocca project for financial support during his visit to MIT. A.E.D. was supported by a National Aeronautics and Space Administration Space Technology Research Fellowship (award no. NNX14AL48H). A.N.M. was supported by a fellowship from the National Science Foundation iQuISE program (award no. 0801525).

## Author contributions

Q.-Y.Z. and K.K.B. came up with the initial idea. Q.-Y.Z. designed and fabricated the nanowire imager. Q.-Y.Z. and D.Z. took the optical measurements. Q.-Y.Z., N.C., F.B. and H.-Z.W. characterized initial devices. A.E.D. developed the superconducting films. Q.-Y.Z., A.N.M. and D.F.S. did the microwave simulations. Q.-Y.Z. analysed the data and programmed the imaging script. K.K.B. supervised the project. Q.-Y.Z. and K.K.B. wrote the paper with input from all the other authors.

## Additional information

Supplementary information is available in the online version of the paper. Reprints and permissions information is available online at [www.nature.com/reprints](http://www.nature.com/reprints). Publisher's note: Springer Nature remains neutral with regard to jurisdictional claims in published maps and institutional affiliations. Correspondence and requests for materials should be addressed to K.K.B.

## Competing financial interests

The authors declare no competing financial interests.

## Methods

**Device fabrication and imaging-pattern preparation.** The SNSPI was fabricated from a ~7 nm thick niobium nitride (NbN) thin film. The film was deposited on a 4 inch (10.16 cm) silicon wafer with a 300 nm thick surface layer of silicon dioxide. The NbN had a critical temperature of  $T_C = 10$  K, a sheet resistance of  $R_s = 331 \Omega \square^{-1}$  at room temperature and a residual resistance ratio of  $\rho_{RRR} = 0.8$ . The kinetic inductance per square was  $L_\square = hR_s/(2\pi^2\Delta\tanh(\Delta/2k_B T)\rho_{RRR}) = 64 \text{ pH } \square^{-1}$ , where  $\Delta = 1.76k_B T_c \tanh(1.74\sqrt{(T_c/T - 1)})$  is the temperature-dependent superconducting energy gap at temperature  $T = 4.2$  K,  $h$  is the Planck constant and  $k_B$  is the Boltzmann constant<sup>34</sup>. The structure of the nanowire transmission line and the tapers were patterned by using a 125 kV electron-beam lithography tool and then transferred into the NbN layer in a CF<sub>4</sub> atmosphere using a reactive ion etcher (more fabrication details are reported in previous publications on SNSPDs<sup>35,36</sup>).

Two objects were imaged with the SNSPI. The object used to generate Fig. 1c was a stainless-steel mesh (McMaster-Carr part number 34735K69) with an opening size of 43 μm and a wire diameter of 30 μm. The structure of the MIT logo image (Fig. 2d) was patterned by using photolithography from a lift-off process on an indium tin oxide (ITO) substrate. The letters were made from a bilayer of metals (50 nm thick chromium and 50 nm thick gold). For each measurement, we placed the object on top of the device with a gap of about 200 μm between the mask and the device. The bias and amplification electronics, which are similar to those used for reading conventional SNSPDs, are all at room temperature. The details of the imaging set-up and electronic configuration are discussed in the Supplementary Information.

**Microwave design of the SNSPI.** We calculated the impedance and velocity of a superconducting transmission line both numerically and analytically. In the analytical calculation, we first calculated the capacitance and inductance of a conventional CPW made from lossless metal and then replaced the inductance with the total of the kinetic inductance and the geometrical inductance. As shown in Supplementary Fig. 1a, both methods showed similar values.

We used the Klopfenstein taper for transforming the nanowire impedance to 50 Ω to preserve the fast-rising edge of a photon-detection pulse. To verify the taper's performance, we fabricated a 17 mm long NbN taper without a photon-sensitive nanowire at the middle. The taper was designed into a CPW structure with a fixed 3 μm gap to the ground plane and a signal line whose width smoothly changed from 88 μm at the two ends to 10 μm in the centre. To characterize the superconducting taper without switching it to the normal state by the input signals, the narrowest width of the nanowire in the centre was designed to 10 μm to have a switching current ( $I_{sw}$ ) of 0.4 mA.

The bandwidth of the taper was measured by a network analyser (Supplementary Fig. 1b). The pass band of the taper started at 0.7 GHz, and was able to cover the spectrum of the fast edge triggered by photon absorption. The performance of the taper also validated the calculation of the superconducting transmission line. Although the pass band stopped at 2.4 GHz because of the loss of the printing circuit board (PCB) and the bonding wires, the bandwidth was sufficient to support the readout of the fast output pulses.

We demonstrated the pulse propagation by sending a pulse into the taper and measuring the output pulse from the other end. A 200 ps wide electrical pulse (Avtech, AVMP-2-C-P-EPIA) was split into two. One pulse was acquired by a 6 GHz oscilloscope as a timing reference while the other pulse was fed into the taper and its transmitted signal was acquired by another channel of the oscilloscope. We also compared the transmitted signal from the taper to the transmitted signal from a 50 Ω transmission line with the same length (corresponding to a delay of 94 ps), but made on a PCB. The delay difference between a PCB transmission line and the taper was 760 ps, which indicates the superconducting taper slowed down the average velocity to 11% of a PCB transmission line. The amplitude of the transmitted signal from a taper reduced to 60% of the transmitted signal from the PCB transmission line; however, the rising edge of the pulse was well preserved, which verifies that the taper helped the propagation of the fast pulse through a wire of mismatched impedance.

In the SNSPI used for taking images, the taper on each end was designed to have a bandwidth whose band pass started at 0.8 GHz. Each taper has an overall length of 27 mm, with its width smoothly changing from 105 μm to 300 nm. As shown in Fig. 2a, the rising edge of the photon-detection pulses was about 240 ps without any reflection, which ensures precise measurements of the delay times  $\tau_1$  and  $\tau_2$ .

**Imaging-processing algorithm.** The raw imaging data were derived from the histogram of differential time,  $\Delta t = \tau_2 - \tau_1$ , of photon counts acquired by the oscilloscope. The purpose of the image processing was to map the photon count  $C_n$  at each time bin  $\Delta t_n$  to the intensity  $I_n$  at the corresponding 2D locations ( $H_n, V_n$ ). First, we calculated the position along the nanowire  $x_n$  from the layout of the double-meandered nanowire, taking into account the effective length of the corner (the corner's effective length was chosen to be 0.68 of its physical length based on numerical simulation of the propagation time through a corner) so that we determined a look-up table mapping  $x_n$  to  $(H_n, V_n)$ . Second, we interpolated the histogram data with a finer time step of 0.045 ps and then converted  $\Delta t_n$  into  $x_n$  by using the formula  $x_n = (\Delta t_n \times v + L_e)/2$ , where  $v = 5.56 \mu\text{m ps}^{-1}$  was the velocity and  $L_e = 17.635 \text{ mm}$  was the effective length. Thus, we were able to map  $t_n$  for each  $C_n$  to  $x_n$ . Finally, we set a 2D image frame with grid sizes of 0.5 μm in both directions, where the 2D locations  $(H_n, V_n)$  were sorted. For each  $(H_n, V_n)$ , the intensity was set to  $C_n$  with a corresponding  $t_n$  and  $x_n$ . To reduce the mapping time, we spread  $C_n$  along the meandered nanowire at  $(H_n, V_n)$  in the 2D image, where the photon counts were distributed according to a Gaussian weight function with a standard deviation of 5 μm. During the mapping process, we shifted  $t_n$  with a constant time to correct for the difference of the delays from electrical connections to the two ends of the wire, and adjusted the velocity to result in a better image quality. The success of the tuning was evaluated by checking the alignments of neighbouring rows.

Instead of using the histogram data, the image can be also constructed from a compilation of single-photon-detection events to offer a real-time single-photon video. To use the same image algorithm discussed previously, raw data of  $(\Delta t, 1)$  was used, with each time difference assigned to one photon count. Supplementary Movie 1 shows a demonstration of such a video by taking the original differential arrival times from the oscilloscope.

**Maximum counting rate of the SNSPI.** The imaging time was limited by the counting rate of the SNSPI and the acquisition speed of the readout. In our present set-up, we used a 6 GHz real-time oscilloscope because of its sub-picosecond intrinsic timing jitter. However, the oscilloscope had a refresh rate of ~100 waveforms per second, which was the bottleneck that limited the overall imaging time. To investigate the ultimate speed of the SNSPI, we ignored the timing information of the pulse and counted pulses from the SNSPI using a 200 MHz counter. We defined  $CR_{max}$  as the count rate when the average detection efficiency dropped by half. As shown in Supplementary Fig. 2,  $CR_{max}$  was  $2 \times 10^6 \text{ c.p.s.}$  measured for 1.5 μm photons. The measured  $CR_{max}$  indicated that the imaging time for an image such as those shown in Fig. 1c and Fig. 2d would be a few seconds if the oscilloscope bottleneck was removed by using a faster readout. The measured  $CR_{max}$  was lower than that of typical SNSPDs because it had a higher total kinetic inductance (estimated to be  $\sim 3 \mu\text{H}$  because of the long wire and the tapers), increasing the time for the current on the nanowire to recover to the initial bias level<sup>8</sup>.  $CR_{max}$  could be increased by incorporating series resistors at each end of the nanowire<sup>20</sup>.

**Data availability.** The data that support the plots within this paper and other findings of this study are available from the corresponding author on reasonable request.

## References

34. Annunziata, A. J. *et al.* Tunable superconducting nanoinductors. *Nanotechnology* **21**, 445202 (2010).
35. Najafi, F. *et al.* Fabrication process yielding saturated nanowire single-photon detectors with 24-ps jitter. *IEEE J. Sel. Top. Quantum Electron.* **21**, 1–7 (2015).
36. Yang, J. *et al.* Fabrication development for nanowire GHz-counting-rate single-photon detectors. *IEEE Trans. Appl. Supercond.* **15**, 626–630 (2005).

## Corrigendum: Single-photon imager based on a superconducting nanowire delay line

Qing-Yuan Zhao, Di Zhu, Niccolò Calandri, Andrew E. Dane, Adam N. McCaughan, Francesco Bellei, Hao-Zhu Wang, Daniel F. Santavicca and Karl K. Berggren

*Nature Photonics* **11**, 247–251 (2017); published online 27 March 2017; corrected after print 14 August 2017.

In the version of this Article originally published, in Fig. 3c, in the *y* axis label, the units '(c.p.s.)' should not have been included; the label should have read "Dark counts". This has now been corrected in the online versions of the Article.